Energy & Environmental Science

COMMUNICATION

View Article Online
View Journal | View Issue

Cite this: *Energy Environ. Sci.*, 2016, **9**, 892

Received 4th December 2015,
Accepted 8th January 2016

DOI: 10.1039/c5ee03655k

www.rsc.org/ees

570 mV photovoltage, stabilized n-Si/CoO_x heterojunction photoanodes fabricated using atomic layer deposition†

Xinghao Zhou,[ab] Rui Liu,[a] Ke Sun,[ac] Kimberly M. Papadantonakis,[ac] Bruce S. Brunschwig[ad] and Nathan S. Lewis*[acde]

Heterojunction photoanodes, consisting of n-type crystalline Si(100) substrates coated with a thin ~50 nm film of cobalt oxide fabricated using atomic-layer deposition (ALD), exhibited photocurrent-onset potentials of −205 ± 20 mV relative to the formal potential for the oxygen-evolution reaction (OER), ideal regenerative solar-to-O_2(g) conversion efficiencies of 1.42 ± 0.20%, and operated continuously for over 100 days (~2500 h) in 1.0 M KOH(aq) under simulated solar illumination. The ALD CoO_x thin film: (i) formed a heterojunction with the n-Si(100) that provided a photovoltage of 575 mV under 1 Sun of simulated solar illumination; (ii) stabilized Si photoanodes that are otherwise unstable when operated in aqueous alkaline electrolytes; and, (iii) catalyzed the oxidation of water, thereby reducing the kinetic overpotential required for the reaction and increasing the overall efficiency relative to electrodes that do not have an inherently electrocatalytic coating. The process provides a simple, effective method for enabling the use of planar n-Si(100) substrates as efficient and durable photoanodes in fully integrated, photovoltaic-biased solar fuels generators.

Broader context

Photoelectrochemical water splitting is an attractive method for converting solar energy directly into hydrogen fuel. However, small-band-gap semiconductors undergo corrosion or passivation reactions in most aqueous electrolytes, especially while oxidizing water to produce O_2(g). Various protection schemes have been developed that allow the use of such semiconductors as photoanodes, but these approaches generally rely on formation of an underlying buried p–n junction to obtain a high photovoltage. High quality emitters or heterojunctions can not however be formed on many semiconductors, and formation of an emitter introduces additional complexity into the fabrication process. We demonstrate herein the use of a thin layer of CoO_x formed by atomic-layer deposition to form a high photovoltage, stabilized photoanode for water oxidation on planar, crystalline n-Si electrode surfaces, demonstrating the possibility of utilizing interfacial engineering to obtain high performance stabilized electrodes without formation of a buried diffused junction. The work provides a demonstration of a simple, scalable process for formation of scalable photoanodes for use in integrated solar fuels generators.

The sustainable electrochemical production of fuels from aqueous electrolytes, accomplished either by reducing water to generate H_2(g) or by reducing CO_2(g) and water to generate hydrocarbons, requires the concomitant oxidation of water to O_2(g), to liberate the electrons needed for the fuel-forming reactions.[1–4] Efficient, intrinsically safe solar-driven water-splitting systems can be constructed in strongly alkaline or strongly acidic electrolytes.[5–7] Such electrolytes also allow the use of commercially available, gas-impermeable, ion-exchange membranes, which have been developed for fuel cells and electrolyzers that use acidic or alkaline electrolytes.[8]

Protective coatings can stabilize technologically important small-band-gap semiconductors for use as oxygen-evolving photoanodes, even in strongly alkaline electrolytes. At least four types of protective coatings have been developed:[9,10] TiO_2, either in an insulating form as a thin (few nm thick) insulating tunnel barrier or in a "leaky" form as a thick (multiple tens of nm) anodically conductive barrier;[11–16] thin metallic coatings;[3] and p-type transparent, conductive transition-metal oxides.[13,17–21] In addition to serving as a physical barrier between the semiconductor and electrolyte, the protective coating should provide high interfacial charge-transfer rates and either be inherently catalytic for the oxygen-evolution reaction (OER) or should support an active OER electrocatalyst, to reduce the kinetic overpotential required for the reaction as well as to assist in the removal of reactive photogenerated holes from the surface of the semiconductor.[22,23] Protective coatings have been demonstrated to extend the lifetime of photoanodes fabricated from semiconductors such as Si, InP,

[a] *Joint Center for Artificial Photosynthesis, California Institute of Technology, Pasadena, CA 91125, USA. E-mail: nslewis@caltech.edu*
[b] *Division of Engineering and Applied Science, Department of Applied Physics and Materials Science, California Institute of Technology, Pasadena, CA 91125, USA*
[c] *Division of Chemistry and Chemical Engineering, California Institute of Technology, Pasadena, CA 91125, USA*
[d] *Beckman Institute and Molecular Materials Research Center, California Institute of Technology, Pasadena, CA 91125, USA*
[e] *Kavli Nanoscience Institute, California Institute of Technology, Pasadena, CA 91125, USA*

† Electronic supplementary information (ESI) available. See DOI: 10.1039/c5ee03655k

and CdTe, which can form surface layers of insoluble, passivating oxides during operation.[13,18]

Integration of protection layers into efficient photoanodes generally has required deposition of the protection layer on top of a homogeneous np^+ buried junction.[13,18,24] However, high quality emitters or heterojunctions can not be formed on many semiconductors. Furthermore, formation of diffused junctions on inexpensive, small-grain-size, polycrystalline or thin-film semiconductors generally results in preferential migration of dopants down the grain boundaries, and thus produces deleterious minority-carrier recombination and majority-carrier shunts in the resulting device.[25]

CoO_x is an electrocatalyst for the evolution of O_2(g) from aqueous alkaline solutions,[26,27] and has been explored as a protective coating for photoanodes.[10,19,28] CoO_x protective layers have been reported to provide only limited stability (a few hours or less) against corrosion for photoanodes in strongly alkaline solutions,[10,28] or require substrates with homogeneous np^+ buried junctions to produce high photovoltages (see ESI† for definition of photovoltage).[19] Recently, deposition of a thin (~2 nm) film of cobalt oxide (CoO_x) prior to the sputter deposition of a multifunctional and protective NiO_x coating onto n-Si surfaces has yielded photoanodes with an electrochemical performance that approaches the Shockley diode limit for the substrate. The interfacially engineered n-Si/$SiO_{x,RCA}$/CoO_x/NiO_x structure demonstrates the fabrication of a stable and efficient device that utilizes a direct heterojunction contact between an n-Si substrate and a protective coating, thereby obviating the need for homogeneous np^+ buried junctions in this system.[29]

We demonstrate herein that stable, high-photovoltage anodes for the oxidation of water from strongly alkaline electrolytes can be fabricated from n-Si substrates protected by a uniform layer of CoO_x formed using atomic-layer deposition (ALD). The ability to fabricate a stable photoanode by deposition of a protective and electrocatalytic coating directly onto a planar substrate without sacrificing device efficiency simplifies the fabrication processes needed to obtain efficient and stable photoanodes for solar-driven water oxidation on Si surfaces. Although the interfacially engineered n-Si/$SiO_{x,RCA}$/CoO_x/NiO_x device provides increased solar-to-O_2(g) conversion efficiency relative to an n-Si photoanode protected by a multi-functional layer of ALD CoO_x, the n-Si/$SiO_{x,RCA}$/CoO_x photoanodes exhibited a lower decay rate of their solar-to-O_2(g) conversion efficiency than n-Si/$SiO_{x,RCA}$/CoO_x/NiO_x photoanodes due to a compact and uniform ALD CoO_x protection layer, along with a simplified fabrication process including lower temperature and fewer processing steps.

Detailed experimental procedures are provided in the ESI.† Briefly, planar Si(100) substrates (0.1–1 ohm cm resistivity, 525 μm thick) were immersed in a Radio Corporation of America Standard Clean-2 (RCA SC-2) etchant for 10 min at 75 °C. This procedure resulted in a thin (~2 nm) SiO_x layer on the surface of the Si (Si/$SiO_{x,RCA}$). CoO_x films were deposited *via* ALD onto Si/$SiO_{x,RCA}$ substrates at 150 °C, with each ALD cycle consisting of a 2 s pulse of a cobaltocene precursor, a 10 s N_2(g) purge at a flow rate of 20 cm^3 min^{-1}, a 5 s pulse of ozone, and another 10 s N_2(g) purge. 1000 ALD cycles (~50 nm) of CoO_x deposition produced optimal

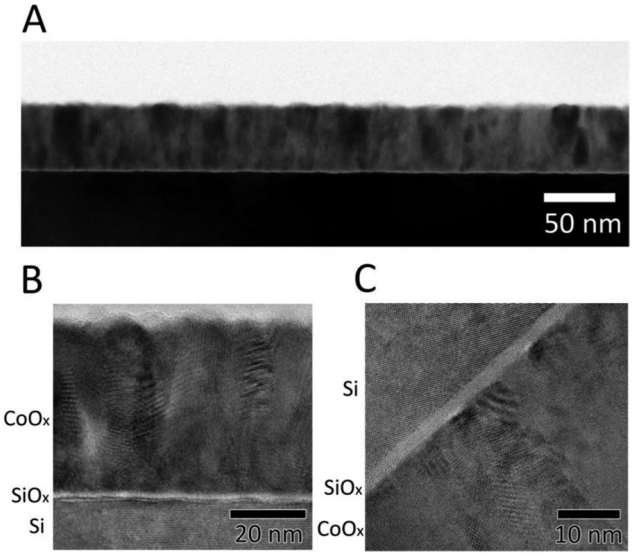

Fig. 1 (A) Low-magnification bright-field transmission-electron micrograph (TEM) of a cross-section of an n-Si/$SiO_{x,RCA}$/CoO_x electrode. (B and C) High-resolution TEM cross-sectional images of an n-Si/$SiO_{x,RCA}$/CoO_x sample. The CoO_x regions show the polycrystalline structure of the CoO_x film.

photocurrent-onset potentials relative to the formal potential for the oxygen-evolution reaction (OER) ($E^{0\prime}$(O_2/H_2O) = 1.23 V *versus* a reversible hydrogen electrode, RHE, at pH = 14) for n-Si/$SiO_{x,RCA}$/CoO_x photoanodes (Fig. S1, ESI†).

Fig. 1A shows a cross-sectional transmission-electron micrograph of the n-Si/$SiO_{x,RCA}$/CoO_x interface collected using bright-field mode. The black region at the bottom of the image corresponds to the Si wafer, the thin bright region atop the Si corresponds to SiO_x, and the polycrystalline layer atop the Si corresponds to the compact CoO_x film, which was uniformly smooth and ~50 nm thick, consistent with the low surface roughness (0.74 nm) determined using atomic-force microscopy (AFM, Fig. S2A, ESI†). Fig. 1B and C show high-resolution transmission-electron microscope (HRTEM) images of the interface. An amorphous SiO_x layer ~2 nm thick was present between the Si substrate and the CoO_x layer, and crystalline grain boundaries were evident in the CoO_x regions of the image. The grain boundaries and in/out-of-plane orientation of the diffraction patterns suggest that the ALD CoO_x films deposited at 150 °C using these methods were polycrystalline rather than amorphous, consistent with results obtained previously using grazing incidence X-ray diffractometry (GIXRD).[29]

Fig. 2A shows typical current-density *versus* potential (*J*–*E*) behavior for n-Si/$SiO_{x,RCA}$/CoO_x photoanodes in contact with 1.0 M KOH(aq), in the dark or under 1.1 Sun of simulated solar illumination provided by a Xe lamp with AM 1.5G filters. The behavior of a nonphotoactive p^+-Si/$SiO_{x,RCA}$/CoO_x electrode is also shown under the same conditions. The light-limited photocurrent density was 30.2 ± 1.1 mA cm^{-2} under these conditions (1.1 Sun illumination), and corresponds to a photocurrent density of ~27 mA cm^{-2} under 1 Sun illumination. Fig. 2B shows the spectral response data (external quantum yield as a function of wavelength) for an n-Si/$SiO_{x,RCA}$/CoO_x photoanode in contact with 1.0 M KOH(aq) while the sample was maintained at 1.93 V *versus* RHE.

When integrated with respect to the spectral irradiance distribution of the AM 1.5G 1.1 Sun solar spectrum, the spectral response of the n-Si/$SiO_{x,RCA}$/CoO_x would be expected to yield a photocurrent density of 30.6 mA cm^{-2}, in good agreement with the light-limited photocurrent observed under 1.1 Sun illumination (see ESI† for detailed calculations).

A representative n-Si/$SiO_{x,RCA}$/CoO_x photoanode exhibited a photocurrent-onset potential of −212 mV relative to $E^{0\prime}(O_2/H_2O)$, 23.2 mA cm^{-2} of photocurrent density at $E^{0\prime}(O_2/H_2O)$, and a solar-to-O_2(g) ideal-regenerative-cell conversion efficiency, η_{IRC}, of 1.5%.[30] With three n-Si/$SiO_{x,RCA}$/CoO_x electrodes tested, the photocurrent-onset potentials were −205 ± 20 mV relative to $E^{0\prime}(O_2/H_2O)$, the photocurrent densities were 22.9 ± 1.6 mA cm^{-2} at $E^{0\prime}(O_2/H_2O)$, and the solar-to-O_2(g) η_{IRC} was 1.42 ± 0.20%. The *J*–*E* behavior of the p^+-Si/$SiO_{x,RCA}$/CoO_x dark electrode provides a measurement of the performance characteristics of the CoO_x layer for the electrocatalysis of O_2(g) production in 1.0 M KOH(aq). A load-line analysis[31] indicated that a photodiode with an open-circuit voltage (V_{oc}) of 575 ± 20 mV, a short-circuit photocurrent density (J_{sc}) of 30.2 ± 1.1 mA cm^{-2}, a fill factor of 0.60 ± 0.01, and a photovoltaic efficiency of η = 11.1 ± 0.5% would be required for a photodiode connected in series with a dark p^+-Si/$SiO_{x,RCA}$/CoO_x anode to exhibit the electrochemical characteristics observed for the n-Si/$SiO_{x,RCA}$/CoO_x photoanode.

Fig. 2C shows the mass of O_2(g) generated as a function of time, as determined using an eudiometer, for an n-Si/$SiO_{x,RCA}$/CoO_x photoanode in contact with 1.0 M KOH(aq). The photoanode was biased to maintain a constant current density of 6.7 mA cm^{-2} (see ESI†), and was illuminated by 100 mW cm^{-2} of AM 1.5G simulated solar illumination. The required bias was 1.6 V and did not change during the 24 h experiment (Fig. S3, ESI†). The mass of O_2(g) that would be produced as a function of time assuming 100% Faradaic efficiency for the oxidation of water to O_2(g) is included as a red curve in Fig. 2C. The measured mass of O_2(g) was within experimental error of the calculated value, indicating that the n-Si/$SiO_{x,RCA}$/CoO_x photoanodes exhibited essentially 100% Faradaic efficiency for the production of O_2(g) under these conditions.

Fig. 2D shows the photocurrent density as a function of time for an n-Si/$SiO_{x,RCA}$/CoO_x photoanode in contact 1.0 M KOH(aq) while biased at 1.63 V *versus* RHE and under 1.1 Sun of ENH-type tungsten-halogen simulated solar illumination. The photocurrent density at 1.63 V *versus* RHE decreased by ∼14% after more than 100 days (∼2500 h) of continuous operation in

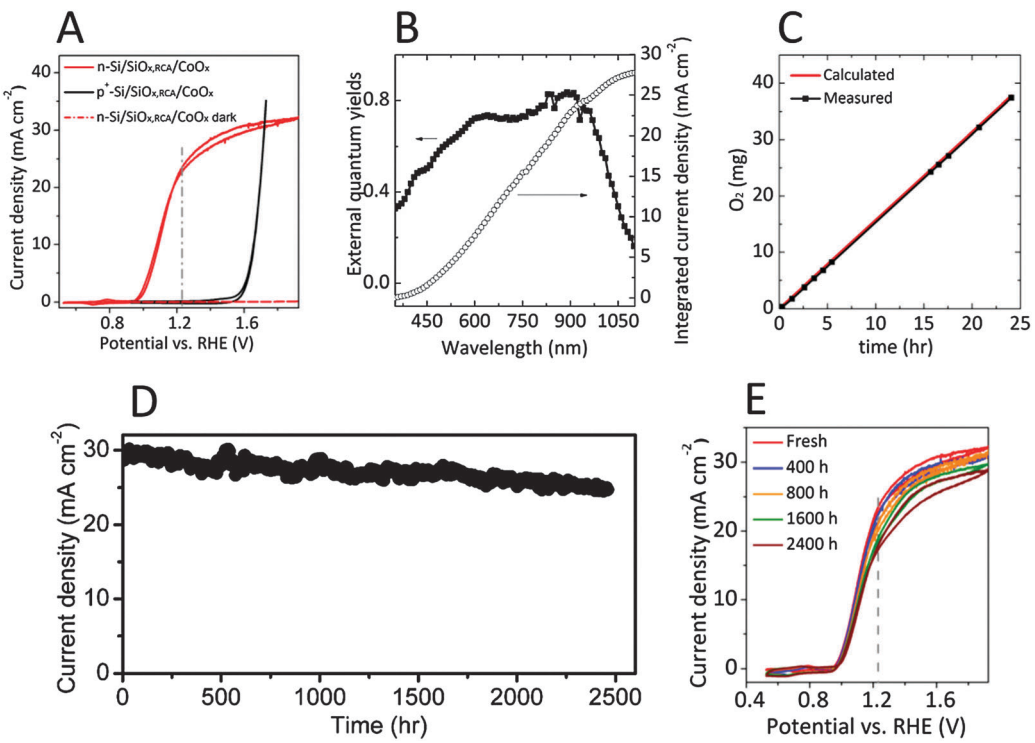

Fig. 2 (A) Representative current-density *versus* potential (*J*–*E*) behavior for n-Si/$SiO_{x,RCA}$/CoO_x photoanodes in contact with a 1.0 M KOH(aq) solution in the dark or under 110 mW cm^{-2} of simulated AM 1.5G solar illumination. The *J*–*E* behavior of a non-photoactive p^+-Si/$SiO_{x,RCA}$/CoO_x electrode is also shown. (B) External quantum yield for an n-Si/$SiO_{x,RCA}$/CoO_x photoanode biased at 1.93 V *versus* a reversible hydrogen electrode (RHE) and in contact with 1.0 M KOH(aq) while illuminated by light that had been passed through a monochromator (left ordinate), and the current density derived by integrating the external quantum yield with respect to the AM 1.5G spectrum (right ordinate). (C) O_2(g) production measured for an n-Si/$SiO_{x,RCA}$/CoO_x photoanode held at a constant current of 6.7 mA cm^{-2} for 24 h while under AM 1.5G simulated illumination and in contact with 1.0 M KOH(aq), and O_2(g) production calculated based on the charge passed assuming 100% Faradaic efficiency (red line). (D) Chronoamperometry of an n-Si/$SiO_{x,RCA}$/CoO_x photoanode held at 1.63 V *vs.* RHE while under 1.1 Sun of simulated solar illumination and in contact with 1.0 M KOH(aq). (E) *J*–*E* behavior of the n-Si/$SiO_{x,RCA}$/CoO_x photoanode as measured periodically during the chronoamperometric stability test shown in (D).

1.0 M KOH(aq), at which point the experiment was terminated but failure of the electrode was not apparent (see ESI,† discussions about stability test). For comparison, the n-Si/$SiO_{x,RCA}$ interface without the CoO_x overlayer showed rapid surface oxidation (Fig. S4A, ESI†). Fig. 2E shows the *J–E* behavior of the photoelectrode as measured periodically during a 100-day stability test. The photocurrent-onset potential relative to $E^{0\prime}(O_2/H_2O)$ increased from −220 mV to −215 mV, −209 mV, −205 mV, and −202 mV, the photocurrent density at $E^{0\prime}(O_2/H_2O)$ decreased from 23.2 mA cm^{-2} to 22.1 mA cm^{-2}, 20.9 mA cm^{-2}, 18.7 mA cm^{-2}, and 17.7 mA cm^{-2}, the photocurrent density at 1.63 V *versus* RHE decreased from 30.4 mA cm^{-2} to 29.7 mA cm^{-2}, 29.2 mA cm^{-2}, 27.8 mA cm^{-2}, and 26.8 mA cm^{-2} and the solar-to-O_2(g) η_{IRC} decreased from 1.47% to 1.40%, 1.27%, 1.15% and 1.05% after 400 h, 800 h, 1600 h and 2400 h, respectively. The decay of the performance might be due to the dissolution of the CoO_x layer, formation of pinholes at the electrode surface (Fig. S2B, ESI†), and the consequent generation of SiO_x islands at the pinholes. The average decay rates of the photocurrent-onset potential relative to $E^{0\prime}(O_2/H_2O)$, the photocurrent density at $E^{0\prime}(O_2/H_2O)$, and the solar-to-O_2(g) η_{IRC} for the n-Si/$SiO_{x,RCA}$/CoO_x photoanode were 7.5 mV, 2.3 mA cm^{-2} and 0.17% per 1000 h, respectively, thus significantly lower than those for the n-Si/$SiO_{x,RCA}$/CoO_x/NiO_x photoanode, which were 36 mV, 7.8 mA cm^{-2} and 0.97% per 1000 h, respectively.[29]

The uniform and compact nature of the ALD CoO_x film may explain the extended stability (~2500 h) and reduced rate of performance decay for these devices in 1.0 M KOH(aq) because the compactness of the film may inhibit the formation of porous CoOOH at the grain boundaries, allowing effective isolation of the Si substrate from contact with the corrosive electrolyte. Also, XPS data (Fig. S5, ESI†) showed the formation of CoOOH at the electrode surface, which could function as an OER catalyst.[32]

Fig. 3A shows the differential capacitance *vs.* potential (Mott–Schottky) data for an n-Si/$SiO_{x,RCA}$/CoO_x photoanode in contact with an aqueous solution that contained the electrochemically reversible, one-electron $Fe(CN)_6^{3-/4-}$ redox couple. The flat-band potential, E_{fb}, calculated from the *x* intercept of the linear region of the data, was −0.85 ± 0.02 V *versus* $E(Fe(CN)_6^{3-/4-})$ (see ESI†), similar to the −0.83 ± 0.02 V *versus* $E(Fe(CN)_6^{3-/4-})$ flat-band potential reported previously for n-Si/$SiO_{x,RCA}$ substrates coated with a thin layer of ALD CoO_x as well as with a 100 nm layer of sputtered nickel oxide.[29] The flat-band potential of the n-Si/$SiO_{x,RCA}$/CoO_x photoanodes is consistent with the presence of significant band bending and therefore with the presence of a large electric field in the space-charge region, which enables efficient separation of photogenerated charge carriers.

The properties of the n-Si/$SiO_{x,RCA}$/CoO_x junction were evaluated further using nonaqueous electrochemical measurements. Fig. 3B compares the photocurrent-onset potentials measured *versus* the Nernstian potential of the solution for n-Si/$SiO_{x,RCA}$/CoO_x photoanodes under 100 mW cm^{-2} of simulated solar illumination and in contact with CH_3CN solutions that contained the one-electron redox couples cobaltocenium/cobaltocene ($Co(Cp)_2^{+/0}$),

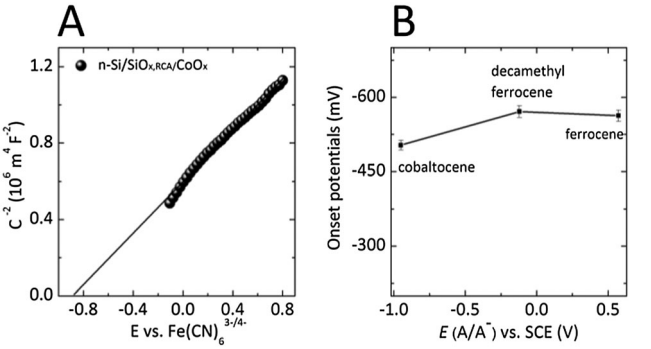

Fig. 3 (A) Mott–Schottky plots of the inverse of the differential capacitance, *C*, of the electrode *versus* potential for an n-Si/$SiO_{x,RCA}$/CoO_x photoanode in contact with a solution of 50 mM $K_3Fe(CN)_6$, 350 mM $K_4Fe(CN)_6$ and 1.0 M KCl aqueous $Fe(CN)_6^{3-/4-}$ (B) Photocurrent-onset potentials *versus* the Nernstian potential of the solution for n-Si/$SiO_{x,RCA}$/CoO_x photoanodes under 100 mW cm^{-2} illumination and in contact with CH_3CN solutions containing the cobaltocenium/cobaltocene, decamethylferrocenium/decamethylferrocene, and ferrocenium/ferrocene redox couples, respectively. The line only connects the experimentally observed values; no functional form is assumed.

decamethylferrocenium/ferrocene ($Me_{10}Cp_2Fe^{+/0}$), and ferrocenium/ferrocene ($Fe(Cp)_2^{+/0}$), respectively. The n-Si/$SiO_{x,RCA}$/CoO_x photoelectrodes exhibited photocurrent-onset potentials of −503 mV, −571 mV, and −563 mV relative to the Nernstian potential of the solution when in contact with $Co(Cp)_2^{+/0}$, $Me_{10}Cp_2Fe^{+/0}$, and $Fe(Cp)_2^{+/0}$, respectively. The variation in photocurrent-onset potentials observed for n-Si/$SiO_{x,RCA}$/CoO_x photoelectrodes was negligible in comparison to the 1.524 V range over which the potential of the contacting solution was varied (−0.951 V for $Co(Cp)_2^{+/0}$, −0.121 V for $Me_{10}Cp_2Fe^{+/0}$ and 0.573 V for $Fe(Cp)_2^{+/0}$ *versus* the saturated calomel electrode (SCE)), indicating that the junction is almost completely buried and therefore unaffected by the Nernstian potential of the solution. These results are consistent with the presence of a compact CoO_x film with few defects that minimize contact between the underlying Si and the solution. In contrast, n-Si/$SiO_{x,RCA}$ substrates coated with 2–3 nm of ALD CoO_x exhibited photocurrent-onset potentials that varied by 510 mV in contact with these same redox species. Additionally, n-Si/$SiO_{x,RCA}$ substrates coated with ~100 nm columnar films of sputtered nickel oxide exhibited photocurrent-onset potentials that varied by 225 mV in contact with the same set of redox couples (Fig. S6, ESI†). These results suggest that 50 nm thick ALD CoO_x films exhibit fewer pinhole-type defects, which allow contact between the underlying Si and the electrolyte, than are exhibited by sputtered NiO_x films, which in turn exhibit fewer through-film defects than thin ALD CoO_x films.

The compact ALD CoO_x layer required an overpotential of 433 mV to drive the OER on p^+-Si at a rate corresponding to a current density of 10 mA cm^{-2} under these conditions. For comparison, under the same conditions, sputtered columnar NiO_x films on p^+-Si require a 330 mV overpotential to produce a current density of 10 mA cm^{-2}.[17] Compared to the n-Si/sputtered-catalyst interface, the n-Si/ALD-catalyst interface was free of detrimental effects produced by the oxygen plasma during the sputtering

process, and was conformal and compact. Assuming that the interface characteristics do not depend on the doping of the substrate, the electrochemical behavior of the p^+-Si anodes can be compared to the photoelectrochemical behavior of the n-Si photoanodes, indicating that the n-Si/$SiO_{x,RCA}$/CoO_x electrodes exhibited both a higher photovoltage and a higher overpotential, by 165 and 103 mV, respectively, relative to n-Si photoanodes protected by a columnar NO_x film. Hence, although an n-Si photoanode with an ALD CoO_x layer exhibited higher solar-to-O_2 conversion efficiency than an n-Si/$SiO_{x,RCA}$/NiO_x photoanode,[29] the interfacial-energetics control of the photovoltage provided by n-Si/$SiO_{x,RCA}$/CoO_x heterojunctions, in combination with the active OER electrocatalysis and protection provided by the NiO_x overlayer, provides a superior combination of properties for a Si heterojunction photoanode effecting water oxidation in alkaline electrolytes.

Prior work involving atomic-layer deposition of CoO_x films ($\sim$4–5 nm thick) onto planar np^+-Si substrates concluded: (i) that such devices are characterized by significant corrosion and a decline in *J–E* response after 30 min of operation in contact with 1.0 M NaOH(aq) while biased at 1.6 V *versus* RHE and under 1 Sun illumination; and (ii) that nanoscale texturing of the substrate surface prior to deposition of the CoO_x film improved both the performance and the stability of devices.[19] For comparison, a CoO_x film was deposited herein onto a planar n-Si/$SiO_{x,RCA}$ photoanode using 100 ALD cycles (n-Si/$SiO_{x,RCA}$/100C-CoO_x, CoO_x film 4–5 nm thick). When operated in contact with 1.0 M KOH(aq) under 1 Sun of simulated illumination, the n-Si/$SiO_{x,RCA}$/100C-CoO_x device yielded a photocurrent density of 20.0 mA cm^{-2} at $E^{0\prime}(O_2/H_2O)$ and a light-limited current density of 27.3 mA cm^{-2} (Fig. S7, ESI†). The performance of the n-Si/$SiO_{x,RCA}$/100C-CoO_x compared favorably to that reported for the planar and nanotextured np^+-Si/CoO_x photoanodes, which exhibited photocurrent densities of 12 mA cm^{-2} and 17 mA cm^{-2} at $E^{0\prime}(O_2/H_2O)$ and light-limited current densities of 27 mA cm^{-2} and 30 mA cm^{-2} under the same conditions, respectively.[19] An n-Si/$SiO_{x,RCA}$ substrate was additionally coated with a thinner layer of CoO_x ($\sim$2–3 nm thick) that was deposited using 60 ALD cycles (n-Si/$SiO_{x,RCA}$/60C-CoO_x). Fig. S8B (ESI†) shows the initial *J–E* behavior of the n-Si/$SiO_{x,RCA}$/60C-CoO_x, as well as the behavior after the one-hour stability test. No significant corrosion nor decline in *J–E* response was observed, in contrast to prior work on planar np^+-Si/60C-CoO_x devices, which exhibited a decay in performance after 30 min of operation under similar conditions.[19]

Several factors may contribute to the improved performance and stability observed in this work for n-Si/$SiO_{x,RCA}$ substrates coated by ALD CoO_x as compared to prior observations of the behavior of np^+-Si homojunctions coated by ALD CoO_x. The n-Si/$SiO_{x,RCA}$/CoO_x heterojunctions exhibit improved spectral response in the short-wavelength region of the solar spectrum ($<$500 nm) relative to devices with np^+-Si homojunctions, because the heterojunctions do not suffer from the parasitic absorption inherent to a p^+-Si emitter layer. In addition, several differences in the methods for ALD of the CoO_x layer may be important contributors to the differences in observations, particularly with respect to the initiation and adhesion of the ALD film, the uniformity of the resulting CoO_x layer, and the nature of the SiO_x layer at the interface. These factors may include: (i) different oxidants (ozone *versus* oxygen plasma); (ii) different deposition temperatures (150 °C *versus* 300 °C); and, (iii) different preparation of substrates prior to ALD (RCA cleaning leaves a thin SiO_x layer on the surface, relative to HF etching which leaves a hydride-terminated Si surface). In combination with the previously reported behavior of n-Si/$SiO_{x,RCA}$/CoO_x/NiO_x photoanodes, the present work clearly demonstrates that CoO_x films deposited using ALD are capable of providing a basis for high photovoltage, stabilized photoanodes on a variety of Si substrates.

We investigated whether the use of 50 nm ALD CoO_x films could be extended readily to produce stable, high-performance heterojunctions with other semiconductors that could produce self-passivating oxides under anodic conditions, specifically n-CdTe. The n-CdTe/CoO_x photoanode exhibited a photocurrent-onset potential of $\sim$+220 mV relative to $E^{0\prime}(O_2/H_2O)$, and a light-limited current density of $\sim$14 mA cm^{-2}, but produced no light-induced current at $E^{0\prime}(O_2/H_2O)$ in 1.0 M KOH(aq) under 1 Sun of simulated solar illumination. The poor performance of n-CdTe/CoO_x devices might be due to lattice mismatch, energy-band misalignment, absence of a passivation layer analogous to the silicon oxide layer on n-Si, or to detrimental effects of the ozone used during the ALD process. Although the n-CdTe/CoO_x devices exhibited increased stability under oxygen-evolution conditions relative to unprotected n-CdTe devices (Fig. S9, ESI†), loss of performance over time was significant. For example, the current density from the n-CdTe/CoO_x device operated in contact with 1.0 M KOH(aq) and biased to 2.8 V *versus* RHE while under 1 Sun of simulated solar illumination decreased by $\sim$10% over a 200 h period, whereas n-CdTe photoanodes that did not have CoO_x protection layer showed rapid surface oxidation, as expected (Fig. S4B, ESI†).

In conclusion, stable and efficient photoanodes for the oxidation of water to $O_2(g)$ in alkaline aqueous electrolytes can be constructed using heterojunctions between planar n-Si(100) substrates bearing a thin chemically grown oxide layer and a 50 nm thick ALD CoO_x film. The Si/$SiO_{x,RCA}$/CoO_x heterojunction simplifies the processing required to produce high-performance stable Si photoanodes by eliminating the need for homogeneous buried np^+ junctions, nanotexturing, or intermediate interfacial engineering layers. The CoO_x film provides multiple desired functions for fully integrated solar-fuels devices, including a high-energy barrier for charge separation, catalytic activity for the water-oxidation reaction, chemical stability, and structural compactness to enable the long-term operation of Si photoanodes.

Acknowledgements

This work was supported by the Joint Center for Artificial Photosynthesis, a DOE Energy Innovation Hub, supported through the Office of Science of the U.S. Department of Energy under Award Number DE-SC0004993. Atomic-force microscopy and UV-Vis spectroscopy were performed at the Molecular Materials Resource Center (MMRC) of the Beckman Institute

at the California Institute of Technology. This work was additionally supported by the Gordon and Betty Moore Foundation under Award No. GBMF1225.

References

1 J. A. Turner, *Science*, 2004, **305**, 972–974.
2 K. Maeda, K. Teramura, D. Lu, T. Takata, N. Saito, Y. Inoue and K. Domen, *Nature*, 2006, **440**, 295.
3 M. J. Kenney, M. Gong, Y. Li, J. Z. Wu, J. Feng, M. Lanza and H. Dai, *Science*, 2013, **342**, 836–840.
4 N. S. Lewis and D. G. Nocera, *Proc. Natl. Acad. Sci. U. S. A.*, 2006, **103**, 15729–15735.
5 E. A. Hernandez-Pagan, N. M. Vargas-Barbosa, T. H. Wang, Y. X. Zhao, E. S. Smotkin and T. E. Mallouk, *Energy Environ. Sci.*, 2012, **5**, 7582–7589.
6 J. Jin, K. Walczak, M. R. Singh, C. Karp, N. S. Lewis and C. X. Xiang, *Energy Environ. Sci.*, 2014, **7**, 3371–3380.
7 S. Haussener, C. X. Xiang, J. M. Spurgeon, S. Ardo, N. S. Lewis and A. Z. Weber, *Energy Environ. Sci.*, 2012, **5**, 9922–9935.
8 J. R. McKone, N. S. Lewis and H. B. Gray, *Chem. Mater.*, 2014, **26**, 407–414.
9 K. Sun, S. Shen, Y. Liang, P. E. Burrows, S. S. Mao and D. Wang, *Chem. Rev.*, 2014, **114**, 8662–8719.
10 S. Hu, N. S. Lewis, J. W. Ager, J. Yang, J. R. McKone and N. C. Strandwitz, *J. Phys. Chem. C*, 2015, **119**, 24201–24228.
11 S. Hu, M. R. Shaner, J. A. Beardslee, M. Lichterman, B. S. Brunschwig and N. S. Lewis, *Science*, 2014, **344**, 1005–1009.
12 M. F. Lichterman, A. I. Carim, M. T. McDowell, S. Hu, H. B. Gray, B. S. Brunschwig and N. S. Lewis, *Energy Environ. Sci.*, 2014, **7**, 3334–3337.
13 M. R. Shaner, S. Hu, K. Sun and N. S. Lewis, *Energy Environ. Sci.*, 2015, **8**, 203–207.
14 M. T. McDowell, M. F. Lichterman, A. I. Carim, R. Liu, S. Hu, B. S. Brunschwig and N. S. Lewis, *ACS Appl. Mater. Interfaces*, 2015, **7**, 15189–15199.
15 Y. W. Chen, J. D. Prange, S. Duhnen, Y. Park, M. Gunji, C. E. Chidsey and P. C. McIntyre, *Nat. Mater.*, 2011, **10**, 539–544.
16 B. Mei, T. Pedersen, P. Malacrida, D. Bae, R. Frydendal, O. Hansen, P. C. K. Vesborg, B. Seger and I. Chorkendorff, *J. Phys. Chem. C*, 2015, **119**, 15019–15027.
17 K. Sun, F. H. Saadi, M. F. Lichterman, W. G. Hale, H.-P. Wang, X. Zhou, N. T. Plymale, S. T. Omelchenko, J.-H. He, K. M. Papadantonakis, B. S. Brunschwig and N. S. Lewis, *Proc. Natl. Acad. Sci. U. S. A.*, 2015, **112**, 3612–3617.
18 K. Sun, Y. Kuang, E. A. Verlage, B. S. Brunschwig, C. W. Tu and N. S. Lewis, *Adv. Energy Mater.*, 2015, **5**, 1402276.
19 J. Yang, K. Walczak, E. Anzenberg, F. M. Toma, G. Yuan, J. Beeman, A. Schwartzberg, Y. Lin, M. Hettick, A. Javey, J. W. Ager, J. Yano, H. Frei and I. D. Sharp, *J. Am. Chem. Soc.*, 2014, **136**, 6191–6194.
20 L. Chen, J. Yang, S. Klaus, L. J. Lee, R. Woods-Robinson, J. Ma, Y. Lum, J. K. Cooper, F. M. Toma, L. W. Wang, I. D. Sharp, A. T. Bell and J. W. Ager, *J. Am. Chem. Soc.*, 2015, **137**, 9595–9603.
21 K. Sun, M. T. McDowell, A. C. Nielander, S. Hu, M. R. Shaner, F. Yang, B. S. Brunschwig and N. S. Lewis, *J. Phys. Chem. Lett.*, 2015, **6**, 592–598.
22 N. C. Strandwitz, D. J. Comstock, R. L. Grimm, A. C. Nichols-Nielander, J. Elam and N. S. Lewis, *J. Phys. Chem. C*, 2013, **117**, 4931–4936.
23 H. Gerischer, *J. Electroanal. Chem.*, 1977, **82**, 133–143.
24 E. Verlage, S. Hu, R. Liu, R. J. R. Jones, K. Sun, C. Xiang, N. Lewis and J. H. A. Atwater, *Energy Environ. Sci.*, 2015, **8**, 3166–3172.
25 A. Heller, *in Photoeffects at Semiconductor-Electrolyte Interfaces*, American Chemical Society, 1981, vol. 146, ch. 4, pp. 57–77.
26 G. Grube and O. Feucht, *Z. Elektrochem.*, 1922, **28**, 568–579.
27 H. Willems, A. G. C. Kobussen, J. H. W. Dewit and G. H. J. Broers, *J. Electroanal. Chem.*, 1984, **170**, 227–242.
28 M. F. Lichterman, M. R. Shaner, S. G. Handler, B. S. Brunschwig, H. B. Gray, N. S. Lewis and J. M. Spurgeon, *J. Phys. Chem. Lett.*, 2013, **4**, 4188–4191.
29 X. Zhou, R. Liu, K. Sun, D. Friedrich, M. T. McDowell, F. Yang, S. T. Omelchenko, F. H. Saadi, A. C. Nielander, S. Yalamanchili, K. M. Papadantonakis, B. S. Brunschwig and N. S. Lewis, *Energy Environ. Sci.*, 2015, **8**, 2644–2649.
30 R. H. Coridan, A. C. Nielander, S. A. Francis, M. T. McDowell, V. Dix, S. M. Chatman and N. Lewis, *Energy Environ. Sci.*, 2015, **8**, 2886–2901.
31 M. R. Shaner, K. T. Fountaine and H.-J. Lewerenz, *Appl. Phys. Lett.*, 2013, **103**, 143905.
32 J. C. Hill, A. T. Landers and J. A. Switzer, *Nat. Mater.*, 2015, **14**, 1150–1155.